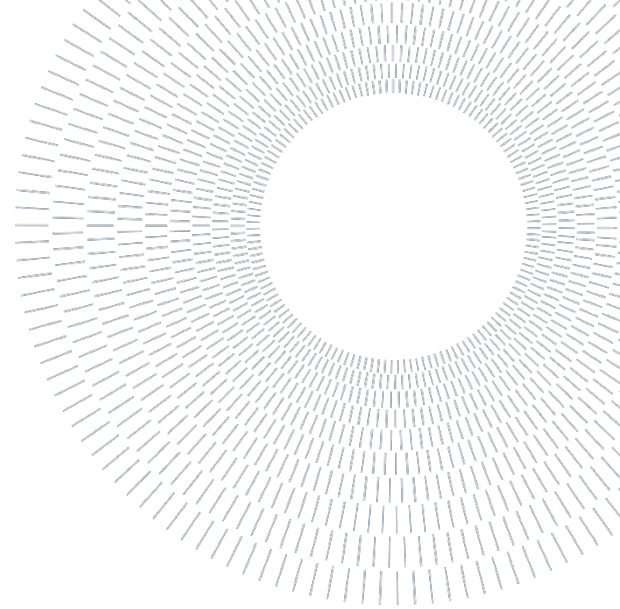




**POLITECNICO**  
MILANO 1863

SCUOLA DI INGEGNERIA INDUSTRIALE  
E DELL'INFORMAZIONE



EXECUTIVE SUMMARY OF THE THESIS

# Design and characterization of fluorinated nanoparticles for CAR-T cell labelling and $^{19}\text{F}$ MRI tracking in glioblastoma therapy

TESI MAGISTRALE IN MATERIALS ENGINEERING AND NANOTECHNOLOGY

**AUTHOR: RAFFAELLA LOBELLO**

**ADVISOR: FRANCESCA BALDELLI BOMBELLI**

**CO-ADVISOR: CRISTINA CHIRIZZI, SERENA PELLEGATTA**

**ACADEMIC YEAR: 2025-2026**

## 1. Introduction

Chimeric Antigen Receptor T-cell (CAR-T) therapy represents a transformative strategy in cancer immunotherapy, leveraging genetically engineered immune cells to recognize and eliminate malignant cells. While CAR-T therapies have achieved remarkable success in hematological malignancies, their application to solid tumors—particularly aggressive brain cancers such as glioblastoma (GB)—remains a major clinical challenge [1]. GB is the most common and lethal primary brain tumor, characterized by infiltrative growth, cellular heterogeneity, and a profoundly immunosuppressive tumor microenvironment, with dismal 2-year survival of 26%–33% [2].

A critical barrier to optimizing CAR-T therapy for solid tumors is the inability to non-invasively monitor the *in vivo* fate of infused therapeutic cells. Key questions regarding their

biodistribution, trafficking to tumor sites, persistence, and correlation with therapeutic response remain largely unanswered. This knowledge gap underscores the urgent need for imaging technologies capable of tracking therapeutic cells in real-time.

Fluorine-19 magnetic resonance imaging ( $^{19}\text{F}$  MRI) has emerged as a particularly promising modality for quantitative cell tracking. The virtual absence of endogenous fluorine in biological tissues provides background-free “hot-spot” detection, where the signal exclusively originates from exogenously administered fluorinated agents. Moreover,  $^{19}\text{F}$  MRI enables quantitative assessment of cell numbers without ionizing radiation and can be implemented on clinical MRI systems [3].

This thesis investigated the development of a fluorinated NP system for labelling CAR-T cells targeting GB, with the aim of establishing a platform for  $^{19}\text{F}$  MRI-based cell tracking. The NPs were formulated using PERFECTA—a superfluorinated molecular probe containing 36 magnetically equivalent fluorine atoms—

encapsulated within biodegradable poly(lactic-co-glycolic acid) (PLGA) and stabilized with sodium cholate (NaC) [4]. The study covered different aspects of the development process, from the physicochemical characterization of the NPs to the optimization of a labelling protocol suitable for CAR-T cells. Following labelling, cell viability, fluorine uptake, and cytotoxic activity against tumoral cells were assessed to verify that the procedure did not compromise the therapeutic potential of the cells.

## 2. Materials and methods

**NPs formulation and characterization.** PERFECTA@PLGA-NaC NPs were formulated by the emulsification solvent evaporation method optimized by Chirizzi et al. [4]. PERFECTA was dissolved in ethyl acetate at elevated temperature and combined with a PLGA solution in the same solvent. The organic phase was added dropwise to an aqueous sodium cholate solution under stirring, followed by tip sonication and prolonged magnetic stirring. The organic solvent was removed by rotary evaporation under gradually decreasing pressure. NPs were then purified by centrifugation and resuspended in Milli-Q water. For fluorescence-based tracking, a 2% of PLGA was replaced with PLGA-Rhodamine B. The resulting colloidal suspension was characterized by dynamic light scattering (DLS),  $^{19}\text{F}$ -NMR, fluorescence spectroscopy and Zeta Potential. The colloidal stability of the NPs was investigated by incubating in culture medium and analyzing temporal changes in size, surface charge, and protein composition.

**Protein Corona Analysis.** NPs were incubated in three different media: T Cell Medium (TCM), TCM conditioned by incubation with CAR T for 6 hours, Milli-Q water (as control). NP-protein complexes were subjected to sedimentation using a sucrose cushion and purified by repeated washing cycles to retain only the hard corona. The adsorbed protein profile was analyzed by SDS-PAGE, while FTIR spectroscopy was employed to confirm protein adsorption through the detection of characteristic amide bands.

**CAR-T cell labelling.** CAR-T cells were generated by lentiviral transduction of peripheral blood T lymphocytes with a CAR construct targeting B7-H3 antigen expressed on GBM cells. The labelling

protocol was systematically optimized across three experimental formats: 24-well plates, 50 mL conical tubes, and T25 culture flasks. Cells were incubated with PERFECTA@PLGA-NaC NPs for 6 hours at a standard fluorine concentration of  $3.13 \times 10^{19}$   $^{19}\text{F}$ /mL, with additional experiments at elevated concentration ( $9.39 \times 10^{19}$   $^{19}\text{F}$ /mL).

**Ficoll purification.** Following incubation, Ficoll density gradient centrifugation was employed to separate labelled cells from free, non-internalized nanoparticles. This purification step was critical to ensure that downstream analytical measurements—particularly  $^{19}\text{F}$ -NMR quantification—reflected exclusively cell-internalized fluorine.

**Viability and cellular uptake.** After Ficoll purification, labelled CAR-T cells were analyzed by flow cytometry (Viability Fixable Dye for viability; rhodamine B fluorescence for uptake quantification),  $^{19}\text{F}$ -NMR spectroscopy (using trifluoroacetic acid as external standard for quantitative determination of cellular fluorine content), and functional co-culture assays with U87 glioblastoma neurospheres at a 1:1 effector-to-target ratio for 3–5 days.

## 3. Results and discussion

### 3.1. NP characterization

PERFECTA@PLGA-NaC NPs exhibited hydrodynamic diameters of 120 nm with PDI below 0.2, confirming monodisperse colloidal systems suitable for cellular uptake. Zeta potential measurements indicated stable surface charge characteristics.  $^{19}\text{F}$ -NMR spectra showed a single sharp resonance peak at  $-72.4$  ppm, corresponding to the 36 magnetically equivalent fluorine atoms of PERFECTA, confirming molecular integrity after encapsulation. Fluorine encapsulation efficiency was consistently high, with approximately 60% of the PERFECTA probe successfully incorporated into the PLGA matrix.

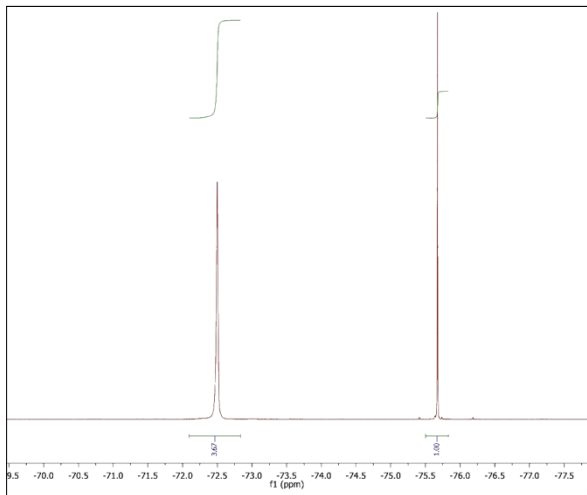


Figure 3.1  $^{19}\text{F}$  NMR spectrum of the NPs. PERFECTA peak ( $-72.4$  ppm) and TFA peak ( $-75.5$  ppm) are visible, with relative integral values used for fluorine atoms quantification.

Protein corona analysis revealed rapid adsorption of serum proteins upon contact with biological medium. DLS stability tests indicated ongoing structural reorganization over 24 hours, with changes in hydrodynamic diameter and surface charge.

SDS-PAGE analysis showed relatively stable protein composition across timepoints, suggesting that reorganization may involve conformational changes rather than wholesale replacement of major corona constituents.

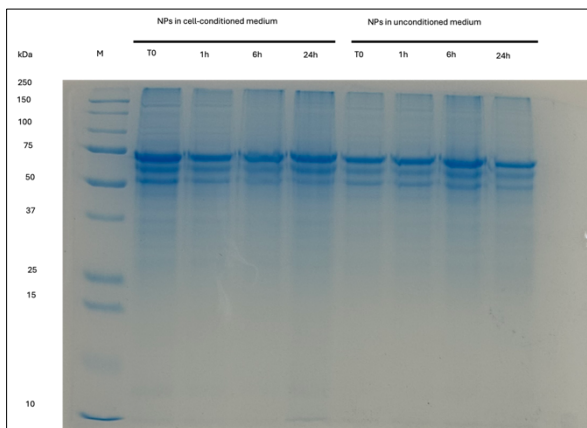


Figure 3.2: 1D SDS-PAGE gel obtained from the hard corona of PLGA-NaC NPs for increasing incubation times (T0 to 24 hours) in cell-conditioned and unconditioned culture medium. Marker proteins column (M) was used to establish the length of protein bands.

FTIR analysis revealed that the characteristic sodium cholate peak appeared shifted and reduced in intensity during incubation in TCM, suggesting progressive protein adsorption onto the NP surface. The shift indicates altered chemical interactions of NaC due to the formation of the

protein corona, while the decrease in peak intensity reflects partial masking of the surfactant layer by adsorbed serum proteins.

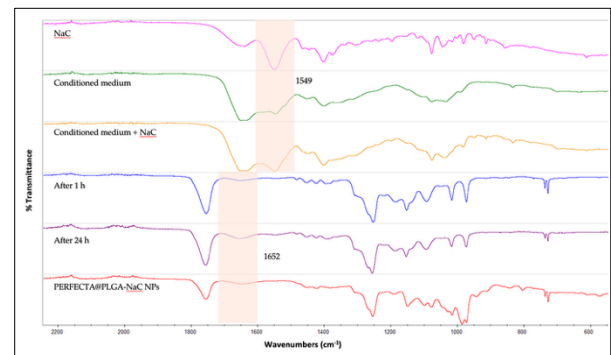


Figure 3.3 FTIR spectra showing the characteristic C=O stretching region. Pure sodium cholate displays a sharp peak at  $1549\text{ cm}^{-1}$ , while sodium cholate incorporated into PLGA nanoparticles shows a broadened peak at  $1652\text{ cm}^{-1}$ .

The combined analysis of DLS, SDS-PAGE, and FTIR data provides a comprehensive picture of protein corona dynamics. While DLS measurements indicated temporal evolution in nanoparticle size and surface properties during protein corona formation, particularly the reorganization observed between early (1 hour) and later (24 hours) timepoints, and SDS-PAGE revealed relatively stable protein composition across timepoints, FTIR demonstrated that the nanoparticle core structure remained intact while showing subtle changes in surface accessibility reflected in peak area variations.

These findings highlighted the importance of evaluating nanoparticle behavior under biologically relevant conditions, as the protein corona may govern biological identity and cellular uptake mechanisms.

### 3.2. *In vitro* experiments with CAR-T

The labelling protocol evolved through three experimental phases. Initial experiments in 24-well plates revealed challenges including partial cell adhesion to plastic surfaces and poor cell recovery. The transition to 50 mL conical tubes mitigated adhesion issues but limited scalability. The final adoption of T25 culture flasks proved optimal by maintaining cells in their standard culture environment—the habitual format for CAR-T cell expansion—while providing sufficient cell yields for comprehensive characterization.

Ficoll density gradient purification was essential for removing free NPs from labelled cell suspensions, as conventional centrifugation-based washing proved inadequate (both cells and NPs co-sediment). While Ficoll achieved complete purification, confirmed by clean  $^{19}\text{F}$ -NMR spectra containing only the cell-internalized PERFECTA signal, it introduced substantial cell losses. Overall recovery rates averaged only  $2.8 \pm 2.7\%$  across T25 flask experiments. Even though this meant losing most of the cells, it was a necessary compromise to obtain clean and reliable data — and it remains the main challenge to address going forward.

### 3.3. Viability and cellular uptake

Flow cytometry demonstrated preserved viability (average  $95.0 \pm 5.9\%$ ) following the labelling and Ficoll purification protocol, confirming biocompatibility. NP uptake was remarkably efficient:  $99.1 \pm 1.3\%$  of cells showed positive rhodamine fluorescence, with near-zero background in control samples (0.004%), indicating true internalization rather than surface adhesion.

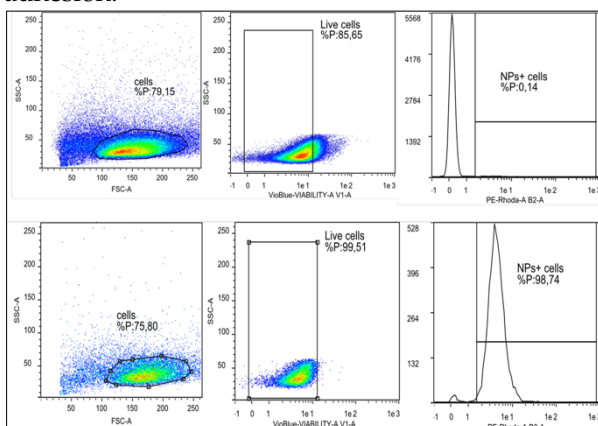


Figure 3.4 Representative flow cytometry analysis of CAR-T cell viability and nanoparticle uptake. Top panels: Unlabelled control cells incubated with Milli-Q water showing high viability and negligible rhodamine background. Bottom panels: CAR-T cells labelled with nanoparticles showing maintained viability and efficient nanoparticle uptake. The rightward shift in rhodamine fluorescence confirms successful nanoparticle internalization without compromising cell viability.

Quantitative  $^{19}\text{F}$ -NMR established an average cellular fluorine loading of  $8.08 \pm 5.36 \times 10^{11}$   $^{19}\text{F}$ /cell at standard concentration across five independent experiments (Table 1). This represents a 4–8 fold improvement over previously published CAR-T cell labelling studies using perfluorocarbon-based agents [5]. Such fluorine content predicts excellent  $^{19}\text{F}$  MRI detectability.

Exp.	Setup	$^{19}\text{F}$ /cell ( $\times 10^{11}$ )	Uptake%	Viab.%	Rhod+%
1	50mL	2.83	0.45	99.96	99.98
2	50mL	3.21	1.53	99.93	96.76
3	50mL	7.93	3.81	97.15	98.97
4	T25	16.5	3.51	88.16	99.88
5	T25	9.91	2.11	89.56	99.71
Avg		$8.08 \pm 5.36$	$2.28 \pm 1.38$	$95.0 \pm 5.9$	$99.1 \pm 1.3$

Table 1: Quantitative  $^{19}\text{F}$  uptake, viability and rhodamine positivity analysis at standard fluorine concentration

Exploratory experiments at elevated fluorine concentration (3-fold increase) demonstrated that cellular loading could reach  $2.25 \times 10^{13}$   $^{19}\text{F}$ /cell—a 28-fold enhancement over standard conditions—while maintaining high viability (97.5%). This disproportionate increase relative to the nanoparticle dose suggests enhanced uptake mechanisms at higher concentrations, though systematic characterization was limited by cell recovery challenges.

### 3.4. Coculture assay

To verify that NP labelling did not impair CAR-T cell function, co-culture experiments were performed with U87 glioblastoma neurospheres at a 1:1 effector-to-target ratio for 3–5 days. Three conditions were compared: non-transduced T cells (NT), unlabelled CAR-T cells (B7-H3 CAR no NPs), and labelled CAR-T cells (B7-H3 CAR NPs+). Flow cytometry analysis (Figure 3.5) revealed that non-transduced T cells failed to eliminate tumor cells, which persisted in the co-culture. In contrast, both unlabelled and labelled CAR-T cells achieved near-complete elimination of GB cells. No appreciable difference in cytotoxic activity was observed between labelled and unlabelled CAR-T cells, confirming that nanoparticle internalization did not compromise therapeutic function.

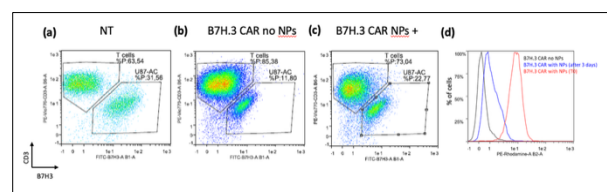


Figure 3.5 Flow cytometry analysis of CAR-T cell cytotoxicity against U87 glioblastoma cells after 3 days of co-culture at 1:1 effector-to-target ratio. (a) Non-transduced T cells co-cultured with U87 cells. (b) B7H3 CAR-T cells without nanoparticles co-cultured with U87 cells (c)

*Nanoparticle-labelled B7H3 CAR-T cells co-cultured with U87 cells. (d) Rhodamine fluorescence overlay.*

It's important to observe the reduction in rhodamine fluorescence intensity during co-culture, likely reflecting CAR-T cell proliferation in response to antigen stimulation. As cells divide, internalized nanoparticles distribute between daughter cells, progressively diluting the per-cell signal. This has important implications for interpreting longitudinal  $^{19}\text{F}$  MRI data, as signal decay may indicate either cell death or successful proliferation—scenarios with opposite therapeutic significance.

## 4. Conclusions

This thesis demonstrated the feasibility of labelling CAR-T cells with PERFECTA@PLGA-NaC nanoparticles for potential  $^{19}\text{F}$  MRI-based cell tracking. The nanoparticle formulation exhibited stable physicochemical properties and high fluorine encapsulation efficiency, while the labelling protocol was progressively adapted to address the specific challenges posed by CAR-T cultures. The optimized procedure achieved a cellular fluorine loading of  $8.08 \times 10^{11}$   $^{19}\text{F}$  atoms per cell, representing a 4–8 fold improvement over published CAR-T labelling studies. Crucially, co-culture experiments with U87 glioblastoma cells confirmed that labelled CAR-T cells retained full cytotoxic activity, demonstrating that the labelling process does not compromise therapeutic function.

Despite these encouraging results, the most significant limitation was the inability to perform  $^{19}\text{F}$  MRI validation due to insufficient cell recovery after Ficoll purification (average overall recovery of ~3%). While the achieved fluorine loadings theoretically predict excellent detectability, experimental imaging confirmation remains essential. Future work should prioritize improving cell recovery through refined Ficoll techniques or alternative purification strategies. Additionally, long-term nanoparticle retention studies and expanded functional characterization would strengthen the translational potential of the approach.

If these technical challenges can be addressed, fluorine-based MRI tracking of CAR-T cells could provide clinicians with a valuable tool to visualize cell distribution, persistence, and tumor infiltration

in vivo, ultimately contributing to the optimization of adoptive cell therapy for glioblastoma and other solid tumors.

## 5. Bibliography

- [1] S. J. Bagley, A. S. Desai, G. P. Linette, C. H. June, and D. M. O'Rourke, "CAR T-cell therapy for glioblastoma: recent clinical advances and future challenges," *Neuro-Oncology*, vol. 20, no. 11, pp. 1429–1438, Oct. 2018, doi: 10.1093/neuonc/noy032.
- [2] O. Netufo *et al.*, "Refining Glioblastoma Surgery through the Use of Intra-Operative Fluorescence Imaging Agents," *Pharmaceuticals*, vol. 15, no. 5, p. 550, Apr. 2022, doi: 10.3390/ph15050550.
- [3] I. Tirota *et al.*, " $^{19}\text{F}$  Magnetic Resonance Imaging (MRI): From Design of Materials to Clinical Applications," *Chem. Rev.*, vol. 115, no. 2, pp. 1106–1129, Jan. 2015, doi: 10.1021/cr500286d.
- [4] C. Chirizzi *et al.*, "Optimization of superfluorinated PLGA nanoparticles for enhanced cell labelling and detection by  $^{19}\text{F}$ -MRI," *Colloids and Surfaces B: Biointerfaces*, vol. 220, p. 112932, 2022, doi: <https://doi.org/10.1016/j.colsurfb.2022.112932>.
- [5] F. Chapelin, S. Gao, H. Okada, T. G. Weber, K. Messer, and E. T. Ahrens, "Fluorine-19 nuclear magnetic resonance of chimeric antigen receptor T cell biodistribution in murine cancer model," *Sci Rep*, vol. 7, no. 1, p. 17748, Dec. 2017, doi: 10.1038/s41598-017-17669-4.